

Magnetic properties and magnon excitations in Fe(001) films grown on Ir(001)T.-H. Chuang,¹ Kh. Zakeri,^{1,*} A. Ernst,^{1,2} Y. Zhang,^{1,3} H. J. Qin,¹ Y. Meng,¹ Y.-J. Chen,¹ and J. Kirschner^{1,4}¹Max-Planck-Institut für Mikrostrukturphysik, Weinberg 2, 06120 Halle, Germany²Wilhelm Ostwald Institut für Physikalische und Theoretische Chemie, Universität Leipzig, Linnestrasse 2, 04103 Leipzig, Germany³Department of Chemistry, University College London, 20 Gordon Street, London WC1H 0AJ, United Kingdom⁴Institut für Physik, Martin-Luther-Universität Halle-Wittenberg, 06120 Halle, Germany

(Received 25 February 2014; revised manuscript received 4 April 2014; published 2 May 2014)

We present a comprehensive study of magnetic properties and high wave-vector magnon excitations in epitaxial Fe(001) films grown on Ir(001) substrate. The magnetic properties are investigated by magneto-optical Kerr effect for various thicknesses of Fe film from 4 up to 27 monolayers. The magnon dispersion relation is obtained by means of spin-polarized electron energy loss spectroscopy. By comparing the experimental and theoretical results, we comment on the effect of the strain induced tetragonal distortion in the Fe film and the electronic hybridizations between the film and the substrate on the exchange interaction and magnon dispersion relation. The thickness-dependent measurements show that the magnon dispersion relation does not change significantly while changing the film thickness in the regime, where the film is uniformly strained. In addition, the measurements are also performed on thicker Fe films, where the films are relaxed into a bulklike structure. The magnon energies close to the zone boundary differ from the ones measured on thick Fe(110) films on W(110). However, the magnon dispersion relation measured for both systems can be well described within the Heisenberg model by using the same effective exchange parameters.

DOI: [10.1103/PhysRevB.89.174404](https://doi.org/10.1103/PhysRevB.89.174404)

PACS number(s): 75.30.Ds, 75.30.Et, 75.70.Rf, 75.50.Bb

I. INTRODUCTION

The investigation of magnetic properties of thin films and surfaces has led to important technological applications, such as giant magnetoresistive read heads or magnetic random access memory (MRAM). The switching time of an MRAM cell is determined by the spin dynamics mechanism. Elementary magnetic excitations, magnons, are the quasiparticles, which describe the spin dynamics in solids. Magnons are also of great importance to understanding the magnetic ordering phenomenon at a finite temperature [1].

Magnetic excitations in ultrathin ferromagnetic films have been studied by ferromagnetic resonance (FMR) [2] and Brillouin light scattering (BLS) [3,4]. However, both methods have the same limitation; only small wave-vector excitations can be investigated. High wave-vector magnons are of particular interest, since they are governed by the exchange interaction and occur on the scales of femtoseconds and nanometers [5–8]. Understanding the spin dynamics in this regime is essential for increasing the density and also the writing/reading speed of modern magnetic data storage devices.

High wave-vector magnons in the bulk Fe have been studied by inelastic neutron scattering (INS) [9,10]. However, due to the weak interaction of neutrons with matter the technique is not appropriate for the investigation of ultrathin films. It has been demonstrated that spin-polarized electron energy loss spectroscopy (SPEELS) [11–13] is a powerful technique to study the high wave-vector magnons in ultrathin ferromagnetic films up to the surface Brillouin zone boundary [14–16]. The technique has already been used to explore the influence of the Dzyaloshinskii-Moriya interaction (DMI) on the magnon dispersion relation [17] and the possibility of tailoring magnetic excitations via changing the atomic structure in low-dimensional ferromagnets [18].

Investigation of high wave-vector magnons in ultrathin Fe films has been limited to Fe(110) films grown on W(110) [15,16,19] and Fe(111) films grown on Au(111)/W(110) [18] and only along one direction (the $\bar{\Gamma}$ – \bar{H} direction). In the SPEELS measurements on the Fe(001)/GaAs(001) system only broad peaks without any obvious dispersion have been observed [20]. For the case of Fe(001)/Ag(001), the measurement has only been performed on a thick [20 monolayers (ML)] Fe film and only a specific wave vector has been measured [21]. The observed peak at relatively high energy region (1–3 eV) is attributed to the exchange splitting. Recently, an EELS investigation on ultrathin Fe films (3–4 ML) on Cu(001) has been reported [22]. It is discussed that the observed magnon signal results from the so-called “nanomartensitic phase” of Fe/Cu(001) with a (1 × 5) reconstruction, caused by the presence of a small dose of hydrogen. Experimentally, the full magnon dispersion relation in Fe(001) films is not known.

Ir(001) is an interesting substrate to study the growth of body-centered cubic (bcc) Fe on a face-centered cubic (fcc) substrate. Its in-plane lattice parameter ($a_{\parallel} = 2.715 \text{ \AA}$) is right in between the corresponding lattice parameters of bcc-Fe (2.866 Å) and fcc-Fe (2.527 Å) [23,24]. Fe(001) films with a thickness from 2 to 10 ML grow pseudomorphically as body-centered tetragonal (bct) structure on Ir(001) substrate with a constant in-plane film strain [25,26]. The room temperature ferromagnetic hysteresis loop has been observed only above 5 ML. Kudrnovský *et al.* have investigated 1 ML Fe on Ir(001) theoretically [27]. They have found out that an unrelaxed 1 ML Fe/Ir(001) has a ferromagnetic ground state but by decreasing the interlayer spacing between the Fe film and the Ir(001) substrate a complex magnetic ground state is observed. Deák *et al.* have also predicted that the magnetic ground state of Fe films on Ir(001) for the film thickness below 4 ML is a complex noncollinear spin structure by including the DMI and biquadratic couplings [28].

*zakeri@mpi-halle.de

Inspired by the previous experimental and theoretical investigations, we carried out measurements on Fe/Ir(001). In this work, we report on the influence of strain induced tetragonal distortion and chemical hybridizations on magnetic properties and in particular on magnetic excitations in this system. In Sec. II, we provide the experimental details and present the results of the structural analysis investigated by low-energy electron diffraction (LEED). In Sec. III A the magnetic properties investigated by magneto-optical Kerr effect (MOKE) on various Fe thicknesses are presented. The magnon dispersion relation in ferromagnetic Fe(001) films grown on Ir(001) is measured by SPEELS. In Sec. III B, the results of magnon excitations in thin films investigated across the onset of room temperature ferromagnetic order (4–5 ML) are presented and discussed. The magnon dispersion relation measured along the [100] direction ($\bar{\Gamma}$ – \bar{X} in the reciprocal space) up to the surface Brillouin zone boundary, on an epitaxial ferromagnetic Fe film with a thickness of 6 ML, is also presented in Sec. III B. In Sec. IV A, by comparing the experimental and theoretical results, we comment on the correlation between the structure and the magnon dispersion relation and the impact of the chemical hybridizations between Fe film and Ir substrate. In Sec. IV B, we discuss the effect of the film thickness on the magnon dispersion relation in the thickness range where the films are ferromagnetic and are uniformly strained (5–10 ML). Finally, we provide and discuss the magnon dispersion relation probed on thick Fe films (19–27 ML), where the films are relaxed to a bulklike structure (Sec. IV C). We also comment on the properties of the films in the intermediate regime (10–19 ML), where the films start to relax from a bct structure to a bcc one.

II. EXPERIMENTS

A. Sample preparation

All the experiments were performed under ultrahigh vacuum (UHV) with the base pressure of $P = 3 \times 10^{-11}$ mbar. Prior to the film deposition the surface of the Ir(001) substrate was prepared using our standard cleaning procedure used for W substrate [29]. By cycles of low power flashes in oxygen atmosphere and a subsequent high power flash in vacuum, carbon is removed from the surface. Since Ir substrate is not strongly reactive to oxygen, carbon is the main contaminant on the Ir surface. Few cycles of low power flashes in oxygen atmosphere ($P_{O_2} = 6 \times 10^{-8}$ mbar) can effectively remove the carbon. The heating power was switched on for 20 s and off for 60 s with an emission current of 65 mA and a voltage of $V = 1.1$ kV ($T \simeq 1500$ K). Then, a single high power flash with an emission current of 140 mA and a voltage of $V = 1.1$ kV ($T \simeq 2000$ K) was used to desorb the oxygen. The LEED pattern of the substrate is shown in Fig. 1(b). The Ir(001) surface usually shows a (5×1) reconstruction. The reconstruction appears in two mutually orthogonal domains. One of the methods to achieve the Ir(001)-(1 × 1) surface is using hydrogen adsorption. With hydrogen adsorption and subsequent annealing, the metastable Ir(001)-(1 × 1) surface structure can be obtained. A detailed recipe has been presented in Refs. [30–32].

The Fe films were grown by molecular beam epitaxy at 300 K. All films were annealed at 900 K to improve the

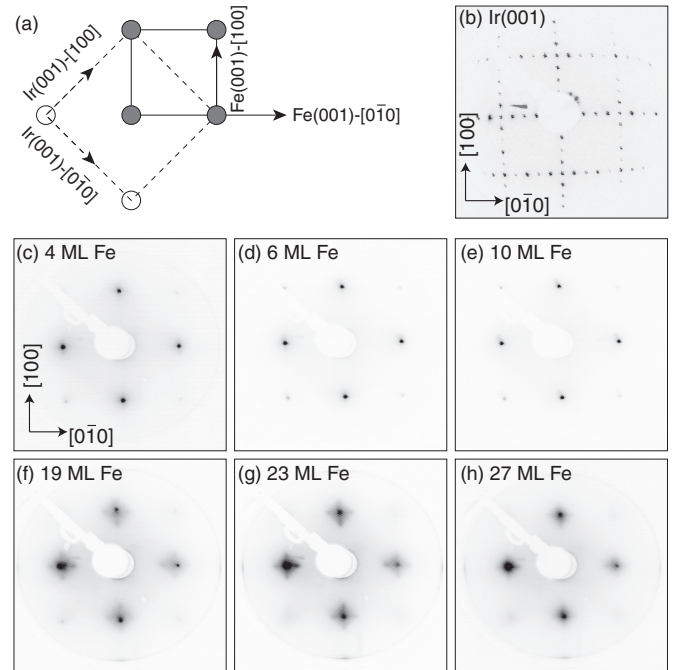


FIG. 1. (a) Schematic representation of the bcc-Fe(001) lattice on fcc-Ir(001). Selection of LEED patterns of (b) Ir(001) with $(5 \times 1 + 1 \times 5)$ surface reconstruction, (c) 4 ML, (d) 6 ML, (e) 10 ML, (f) 19 ML, (g) 23 ML, and (h) 27 ML Fe films grown on Ir(001). All images are taken at a primary electron energy of 100 eV. Before recording the LEED patterns, Fe films are annealed at 900 K.

surface quality. In Figs. 1(c)–1(h), a series of LEED patterns of Fe films with various thicknesses are shown. For films thinner than 10 ML, the patterns are very similar and the diffraction spots are clear and sharp. In agreement with the previous study, the Fe films are pseudomorphically grown up to around 10 ML. With increasing film thickness, extra satellite spots start to appear around the original spots [see Fig. 1(f)]. The satellite spots may originate from the extra periodic arrangement of atoms along the $\langle 100 \rangle$ direction of Fe(001) [the $\langle 110 \rangle$ direction of Ir(001)]. It is also observed that the distance between the main spots is slightly decreased, comparing the patterns presented in Figs. 1(c) and 1(h). It indicates that the lattice parameter is longer when the film is relaxed. This observation is in agreement with the literature reporting a lattice relaxation for films with thicknesses above 10 ML. The interlayer spacings of each Fe layer on Ir(001) have been obtained by structural LEED intensity analysis for 1, 2, 4, and 9 ML Fe [25]. The results are taken as the input parameters for our calculations of magnon dispersion relation (see Sec. IV A).

B. MOKE experiments

The magnetic properties of the films were investigated by means of MOKE. The angle of the incident and scattered laser beam with respect to the film normal was 45° . The measurements were performed in longitudinal geometry at room temperature for Fe films of different thicknesses. The external magnetic field was applied along the Fe $[0\bar{1}0]$ direction. Before the measurements, the sample was annealed at about 900 K to improve the surface quality.

C. SPEELS experiments

The magnetic excitations were investigated by SPEELS. In the SPEELS experiments, spin-polarized electrons are scattered from a sample. The energy and momentum transfer of the scattered electrons are analyzed for the two possible spin directions of the incident electrons. The intensity of the scattered electrons is recorded as a function of their energy loss. Due to the conservation of total angular momentum, only incident electrons of minority character can excite magnons. Such a scattering event is governed by the exchange process. An extended discussion on the process involved in the scattering event can be found in Refs. [8,33–35].

For all experiments presented here, the sample was magnetized along the easy axis before the SPEELS experiments. The measurements were performed in the remanent state. The scattering plane was chosen to be parallel to the Fe[100] direction and the sample was magnetized along the direction perpendicular to that [see Fig. 3(a)].

III. RESULTS

Since Fe(001) films grown on Ir(001) substrate with different thicknesses show very different structural and magnetic properties, here we present and discuss our experimental results within five sections. First, the MOKE results measured on different thicknesses of Fe at 300 K are presented. Then, the results of the SPEELS measurements on different film thicknesses [(i) 4–6 ML, (ii) 6 ML, (iii) 6–10 ML, and (iv) 10–27 ML] are shown and discussed separately.

A. MOKE results

In Figs. 2(a)–2(f), the MOKE hysteresis loops obtained on different thicknesses of Fe are presented. The ferromagnetic hysteresis loop was only obtained when the thickness was above 5 ML. The Kerr ellipticity is plotted for different Fe thicknesses as seen in Fig. 2(g). The black squares represent

the Kerr ellipticity in saturation, and the red circles indicate the one in remanence.

From 5 to 10 ML, a rectangular hysteresis loop is obtained. Starting from 13 to 19 ML, the shape of the loops changes [see Fig. 2(e)]. The S-like loops indicate that the easy magnetization direction is changed. Since we did not observe this feature in the film without annealing, the magnetic anisotropy may be changed due to the annealing of the film. This indicates that the magnetic anisotropy of Fe films in this region from 13 to 19 ML is sensitive to the annealing temperature. When the thickness is above 23 ML, the loops change back to the rectangular ones indicating the easy axis measurement as seen in Fig. 2(f). According to the stress measurements performed by Tian *et al.* [25,26] and also our LEED experiments presented in Fig. 1, in the region of 10 to 20 ML the Fe structure is relaxing from a bct structure to a bcc one. This fact is also revealed in the hysteresis loops. In this region the macroscopic magnetization of the film is no longer parallel to the applied field direction. The saturation magnetization measured by MOKE increases linearly with the film thickness from 5 up to 27 ML. This fact rules out the possibility of having an in-plane to out-of-plane spin reorientation transition in the region of 10–20 ML. For an in-plane to out-of-plane spin reorientation one would expect an abrupt change in the Kerr signal together with a large enhancement of the coercive field. Such a behavior is not observed for Fe films on Ir(001) [see Fig. 2(e)].

Still it is not completely understood why there is no magnetic signal below 5 ML Fe at room temperature (4 ML at low temperature [25]). It would be interesting to investigate the magnon excitations in the transition region, where the thickness is thinner than 5 ML. Since Fe films grow pseudomorphically as bct structure on Ir(001) from 2 to 10 ML [25,26], it is also a great opportunity to measure the magnon dispersion relation on a series of Fe films in the pseudomorphically grown region from 5 to 10 ML and also in the region where the atomic relaxation takes place (thicker than 10 ML).

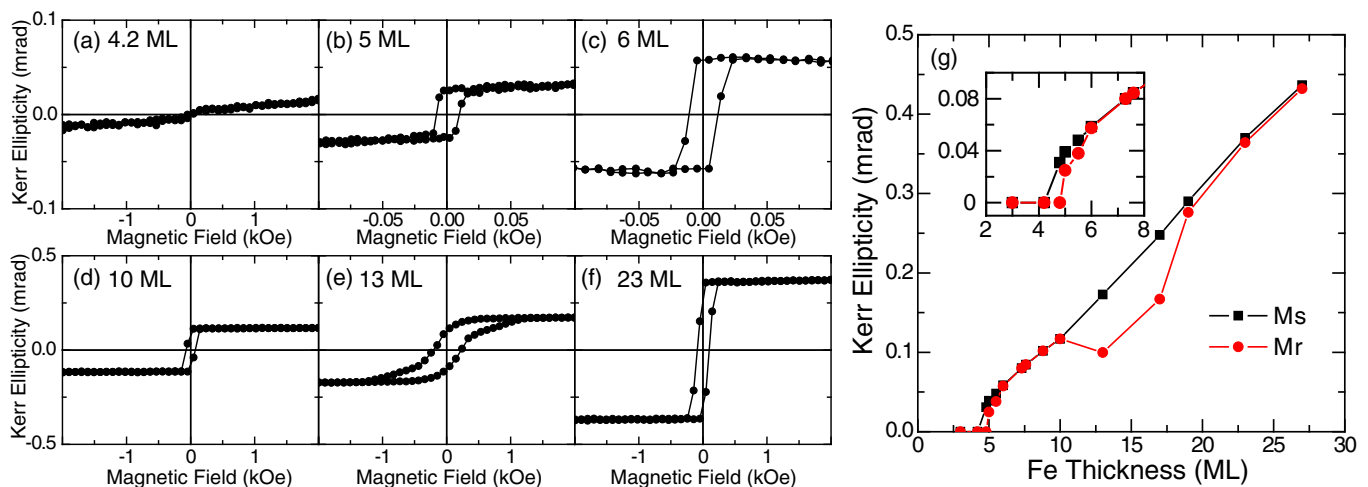


FIG. 2. (Color online) Longitudinal MOKE measurements on Fe films grown on Ir(001) with different thicknesses at 300 K. The hysteresis loops are obtained on (a) 4.2 ML Fe, (b) 5 ML Fe, (c) 6 ML Fe, (d) 10 ML Fe, (e) 13 ML Fe, and (f) 23 ML Fe. All loops are obtained after annealing the sample at about 900 K. The magnetic field is applied along the $[0\bar{1}0]$ direction. (g) Kerr ellipticity as a function of the Fe thickness in saturation (M_s) (black squares) and in remanence (M_r) (red circles). The large difference between M_s and M_r in the region of 10–19 ML is due to the structural relaxation taking place in this region (see the text). Inset shows an enlargement at the scale of thicknesses from 2 to 8 ML.

The results of magnetic excitations probed by SPEELS are presented in the following section.

B. SPEELS results

In Figs. 3(b)–3(d), the SPEEL spectra obtained on 4.2 ML, 4.8 ML, and 5 ML Fe grown on Ir(001) at an in-plane wave-vector transfer of $\Delta K_{\parallel} = 0.8 \text{ \AA}^{-1}$ are presented. The measurements are performed along the Fe[100] ($\bar{\Gamma}-\bar{X}$) direction and at room temperature. The scattering geometry is shown in Fig. 3(a). The incident electron energy was 6 eV with a total energy resolution of 15 meV. I_{\downarrow} (I_{\uparrow}) indicates the intensity of the scattered electrons when incoming electrons have the spin polarization antiparallel (parallel) to the spin of majority electrons in the Fe films. The room temperature ferromagnetic hysteresis loop only appears when the thickness is above 5 ML as seen in Fig. 2. The corresponding results of longitudinal MOKE measurements are shown in the inset. The magnon energies could be more easily identified in the difference spectra ($I_{\downarrow} - I_{\uparrow}$). The peak position indicates the excitation energy. In the difference spectrum, the intensity is almost zero for the measurement on a 4.2 ML Fe film as shown in Fig. 3(b). For the measurement on a 4.8 ML Fe film [see Fig. 3(c)], the I_{\downarrow} channel is slightly deviated from the I_{\uparrow} channel in the energy loss region. In other words, the ferromagnetic magnon signal appears, but the intensity is still very weak. When the thickness reaches 5 ML, a clear shoulderlike feature appears in

the I_{\downarrow} channel in the energy loss region, indicating the evident magnon excitations [see Fig. 3(d)]. A typical ferromagnetic hysteresis loop obtained on 5 ML Fe/Ir(001) is also shown in the inset of Fig. 3(d). The difference spectra obtained on 4.2, 4.8, 5, and 6 ML Fe at $\Delta K_{\parallel} = 0.8 \text{ \AA}^{-1}$ are compared in Fig. 3(e). The magnon energy stays approximately at the same value within our experimental error when it goes across the thickness of room temperature ferromagnetic order (5 ML), but the magnon intensity is largely enhanced. The tail-like feature in the spectra measured on 4.2 and 4.8 ML Fe films may be a signature of the excitations in both channels. As these films show no remanence, such an observation is expected. As soon as one reaches the ferromagnetic order, the loss feature in the I_{\uparrow} channel (blue upward triangles) is strongly suppressed and the one in the I_{\downarrow} channel (red downward triangles) is increased [see Fig. 3(d)]; consequently, the difference intensity is increased. The largely enhanced difference intensity, comparing the 5 and 6 ML samples, results from the fact that the SPEELS measurements are done in the remanence state and the remanent signal is slightly lower than the saturation in the case of 5 ML as seen in the hysteresis loop measured by MOKE.

It should be noted that although no spin-resolved loss features could be observed for the samples with the thickness below 4.8 ML, it does not mean that there are no magnon excitations in those films. Maybe, due to the weak magnon intensity and low magnon energies, they do not show up as well-defined loss features.

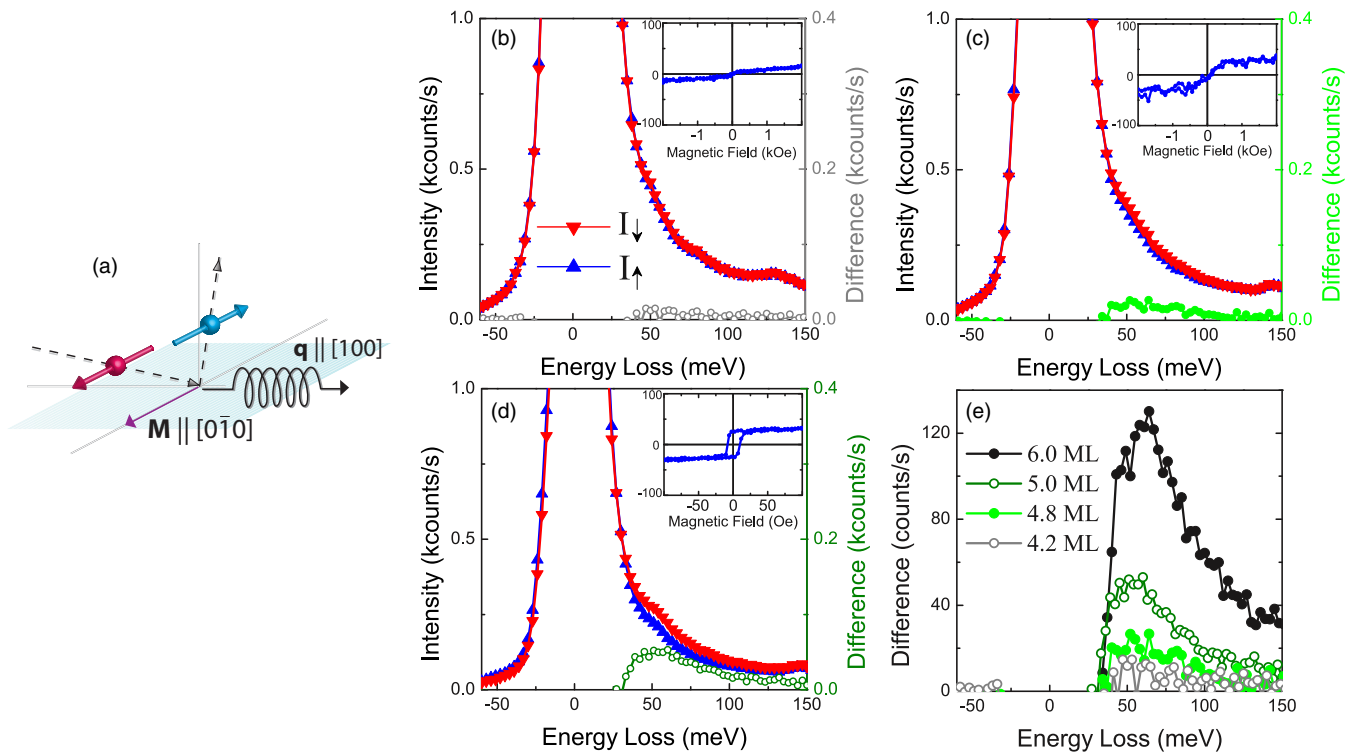


FIG. 3. (Color online) (a) Scattering geometry used for the SPEELS measurements. SPEEL spectra I_{\downarrow} (red), I_{\uparrow} (blue), and their difference for (b) 4.2 ML, (c) 4.8 ML, and (d) 5 ML Fe grown on Ir(001) at an in-plane wave-vector transfer of $\Delta K_{\parallel} = 0.8 \text{ \AA}^{-1}$. The experiments are performed at 300 K. The scattering plane is parallel to the Fe[100] direction. All data are obtained using the incident electron energy of 6 eV with a total energy resolution of about 15 meV. The hysteresis loops obtained by the longitudinal MOKE measurements with the field applied along the $[0\bar{1}0]$ direction are shown in the insets. The y axis of all insets is the Kerr ellipticity in the units of microrad. (e) The difference ($I_{\downarrow} - I_{\uparrow}$) spectra at $\Delta K_{\parallel} = 0.8 \text{ \AA}^{-1}$ for different film thicknesses are plotted together for comparison.

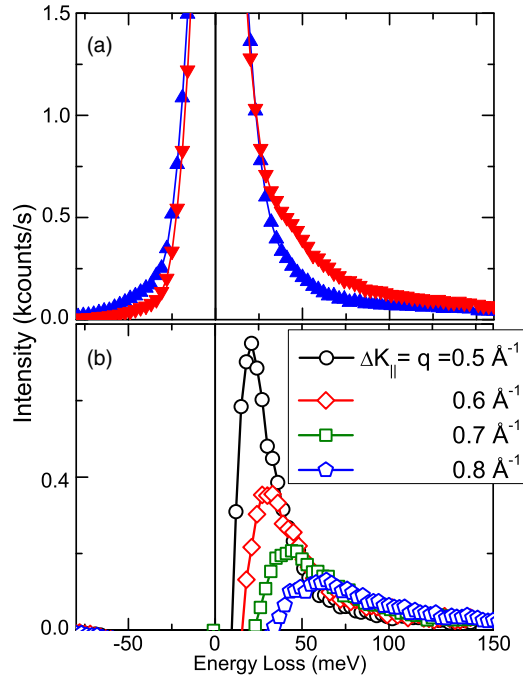


FIG. 4. (Color online) (a) Typical SPEEL spectra recorded on 6 ML Fe/Ir(001) at an in-plane wave-vector transfer of $\Delta K_{\parallel} = 0.7 \text{ \AA}^{-1}$ probed along the Fe[100] direction. The intensity spectrum I_{\downarrow} (I_{\uparrow}) is obtained using the incident electrons with the spin orientation antiparallel (parallel) to the spin of majority electrons in the Fe film. The experiments are performed at 300 K. (b) A series of difference spectra ($I_{\downarrow} - I_{\uparrow}$) at in-plane wave-vector transfers from 0.5 to 0.8 \AA^{-1} probed along the Fe[100]-($\bar{\Gamma}$ - \bar{X}) direction.

In order to understand the effect of strain induced tetragonal distortion and chemical hybridizations on magnetic properties in the following section, we focus on the results of a 6 ML film which shows a typical ferromagnetic hysteresis loop and a well resolved magnon loss feature. Typical SPEEL spectra measured on a 6 ML Fe film grown on Ir(001) at an in-plane wave-vector transfer of $\Delta K_{\parallel} = 0.7 \text{ \AA}^{-1}$ are shown in Fig. 4(a). The incident electron energy was 6 eV with a total energy resolution of 16.9 meV. The magnon peak is pronounced in the energy loss region of the minority channel.

A series of difference spectra with various wave-vector transfers ranging from 0.5 to 0.8 \AA^{-1} are shown in the Fig. 4(b) for the probing direction along the $\bar{\Gamma}$ - \bar{X} direction. The difference spectra show a clear dispersion. By plotting the magnon energies as a function of the wave-vector transfer, the magnon dispersion relation is obtained up to the surface Brillouin zone boundary [see Fig. 5(a)]. The length of $\bar{\Gamma}$ - \bar{X} is 1.16 \AA^{-1} , assuming the in-plane lattice constant of Fe is 2.72 \AA [since Fe grows pseudomorphically on Ir(001) substrate up to 10 ML [25]].

We observed that the magnon dispersion relation for the films with thicknesses of 6–10 ML is nearly the same. We discuss the results of this thickness range in Sec. IV B. The magnon dispersion relation for thicker films was different. A discussion on the measured magnon dispersion relation for thicker films (> 10 ML) is provided in Sec. IV C.

Recently, the theoretical magnon dispersion relation for Fe(001) films on Cu(001) has been calculated by a combination

of first principles calculations and spin dynamics simulation [36]. The calculated energies are by a factor of 2 larger than our experimental values measured for Fe(001) films on Ir(001).

IV. DISCUSSIONS

A. 6 ML Fe

In order to have a better understanding of the system, we performed *ab initio* calculations of magnon dispersion relation. The calculations are performed within the generalized gradient approximation of the density functional theory [37]. The lattice parameters of Fe/Ir(001) were taken from the experimental results by means of the IV-LEED analysis [25]. The in-plane lattice parameter of Fe was the same as the Ir substrate (2.72 \AA). The interlayer distance of Fe-Ir was 1.75 \AA and the interlayer distances of all Fe layers were 1.6 \AA . This information serves as an input for the calculations of electronic and magnetic properties using a self-consistent Green function method, which is designed for layered structures [38]. The interatomic exchange parameters were determined employing the magnetic force theorem, implemented within the Green function method [39].

The calculations performed for 6 ML Fe on Ir(001) are shown in Fig. 5(a) by the green (solid) line. The results of calculations for 6 ML Fe are in good agreement with the experimental results. However, small deviations can be observed, which might be due to the following different reasons. (i) The relativistic effects are not taken into account in the theory. (ii) The interatomic distances for our case might be slightly different from the ones of the literature value, since the Fe film is grown on a reconstructed Ir substrate rather than a (1×1) surface.

In order to understand the role of the electronic hybridizations with the substrate and the atomic relaxation on the magnon dispersion relation, additional calculations are performed for three different cases. In Fig. 5(b), the blue (dashed) line represents the calculated results using the in-plane lattice constant the same as the nearest neighbor atomic distance of Ir(001) (2.72 \AA) but using the Fe bulk value (2.86 \AA) as the vertical lattice constant. This would correspond to a c/a ratio of 1.04. A characteristic change in the energies in the intermediate wave vector is observed when the c/a ratio is changed from 1.16 (solid line) to 1.04 (dashed line). The magnon energies calculated along the $\bar{\Gamma}$ - \bar{M} direction (not shown here) deviate largely from the experimental values.

The light green (dash-dotted) line represents results of the calculations for the free-standing 6 ML Fe with the same input parameters as the green (solid) one (experimental values). There is a huge enhancement of the energy for the free-standing film. This demonstrates that the effect of chemical hybridizations of the Fe film and the Ir substrate on the magnon dispersion relation is of major importance. The gray (dotted) line represents the calculation for a free-standing film with the in-plane and vertical lattice constants of the bulk Fe. The magnon energies are lower than the ones of the distorted free-standing Fe film (light green curve), but much larger than the ones of the Fe films grown on Ir substrate (green and blue curves). Only in the case where all experimental parameters are taken into consideration can one have a good agreement between the experimental data and the calculations.

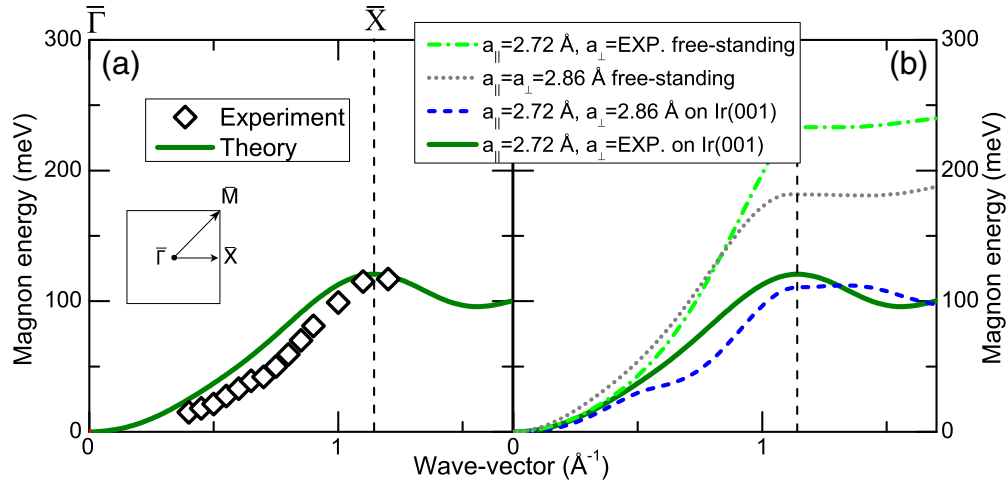


FIG. 5. (Color online) (a) Experimental (open diamonds) and theoretical (solid curve) magnon dispersion relation of 6 ML Fe/Ir(001). (b) The calculated magnon dispersion relation for four different cases: (i) a pseudomorphically grown Fe film on Ir(001) with the vertical lattice constant obtained by IV-LEED measurements [25] (green solid line); (ii) a pseudomorphically grown Fe film on Ir(001) with the vertical lattice constant of the bulk Fe (blue dashed line); (iii) a free-standing Fe film with the experimental lattice constants (light green dash-dotted line); (iv) a free-standing Fe film with the Fe bulk lattice constants (gray dotted line).

Therefore, not only the strain induced distorted lattice structure but also the chemical hybridizations of the Fe films and the Ir substrate influence the magnetic excitations in the Fe film.

In Fig. 6, the calculated site-resolved exchange constants are presented. The results for the case of experimental interlayer spacing are shown in red (filled) symbols and the ones for the bulk interlayer spacing are shown in blue (open) symbols [see Figs. 6(b) and 6(c)]. The results of the free-standing film with the experimental lattice parameters are shown in green (open) symbols [see Figs. 6(d) and 6(e)]. Each case has two sets of exchange parameters, namely *intralayer* (J_{\parallel}) and *interlayer* (J_{\perp}) exchange parameters. The exchange interaction between atoms within the same atomic layer is referred to as intralayer interaction and the one between atoms from different layers is referred to as interlayer interaction, which is depicted in Fig. 6(a). The exchange parameters for the atoms located at the interface of Fe and Ir and the ones located at the surface of Fe are shown in Figs. 6(b) and 6(d) and Figs. 6(c) and 6(e), respectively.

First, we discuss the effect of the chemical hybridizations between the Fe films and the Ir substrate on the exchange interaction. At the Fe surface, the exchange parameters do not differ when the film is grown on Ir or is regarded as a free-standing film [see Fig. 6(e)]. However, at the interface, it is observed that both the inter- and intralayer exchange parameters are substantially smaller for a film grown on the substrate compared to the free-standing film. Especially the intralayer exchange parameters are much smaller in the former case. The intralayer exchange parameters show a relatively weak ferromagnetic coupling compared to the interlayer exchange. The ones close to the Fe/Ir interface are even negative [the red (solid) square in Fig. 6(d)]. Although the couplings have a tendency to be antiferromagnetic in each layer, due to the strong ferromagnetic coupling between the layers, the net magnetic state of this film is still ferromagnetic. This result suggests that 1 ML Fe on Ir(001) is not a simple ferromagnet. We note that the relativistic effects are not considered in these calculations. It has been shown by theoretical calculations

that including relativistic corrections in the case of ultrathin (1 to 4 ML) Fe films on Ir(001) leads to the appearance of complex noncollinear spin structures [28]. However, without

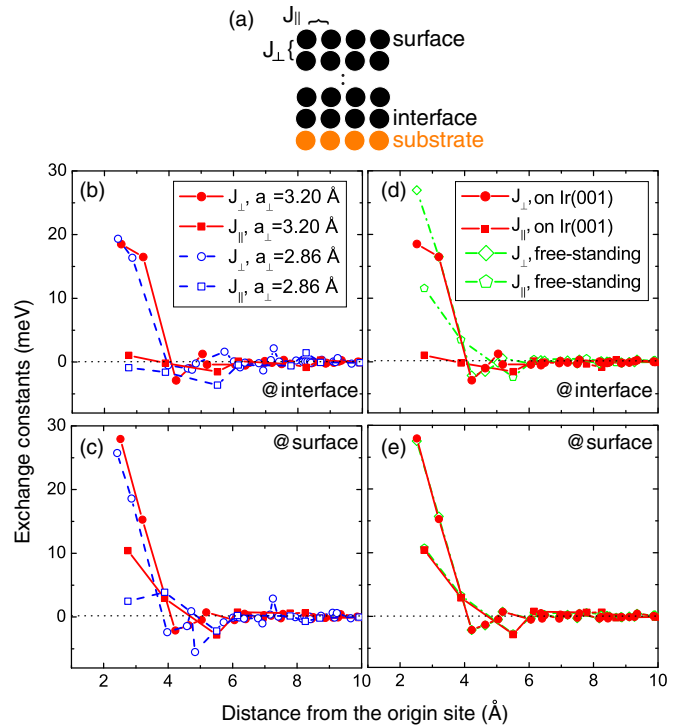


FIG. 6. (Color online) Calculated site-resolved interlayer, J_{\perp} , and intralayer, J_{\parallel} , exchange constants for the atoms located in the interface layer (b),(d) and in the surface layer (c),(e) [the geometry is shown in (a)] for the case of (i) a pseudomorphically grown Fe film on Ir(001) with the vertical lattice constant obtained by IV-LEED measurements [25] (red solid line), (ii) a pseudomorphically grown Fe film on Ir(001) with the vertical lattice constant of bulk Fe (blue dashed line), and (iii) a free-standing Fe film with the experimental lattice constants (green dash-dotted line).

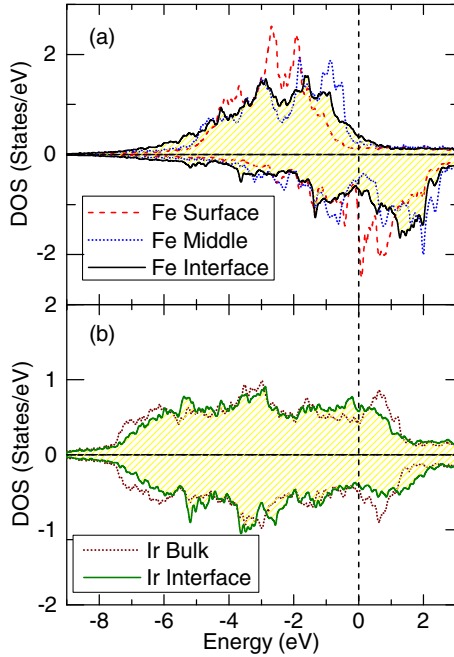


FIG. 7. (Color online) (a) Spin- and layer-resolved density of states of Fe atoms sitting in the surface layer (dashed curve), in the interior of the Fe film (dotted curve), and in the interface Fe layer (solid curve). (b) Spin- and layer-resolved density of states of Ir atoms sitting in the bulk Ir (dotted curve) and in the interface Ir layer (solid curve).

considering the relativistic effects, the theoretical results of the magnon dispersion relation fit quite well to the experiment. It suggests that these effects may not influence the magnon energies too much for these film thicknesses (>5 ML). This is rather expected, since the exchange energy dominates the magnetic energy of the system.

It has been shown that the spectral density of the low-energy magnon mode close to the Brillouin zone boundary is largest at the interface, due to the relatively weak exchange interaction at the Fe/Ir interface [40]. In other words, the main contribution to this magnon mode is coming from the interface layer. This is due to the fact that the exchange interaction at the interface is weaker than at the surface. Moreover, this magnon mode has the longest lifetime among the other magnon modes associated to the other parts of the Fe film. Hence it dominates the measured spectra. Other magnon modes are also present in the system. Since they are heavily damped, they cannot be easily distinguished from the background [40].

In order to shed light on the nature of the interfacial electronic hybridizations in this system, we carefully investigated the layer-, orbital-, and spin-resolved density of states (DOS). The results of the layer-resolved DOS of 6 ML Fe on Ir(001) are summarized in Fig. 7. Here, for simplicity, we present and compare the DOS of atoms sitting in five different places: (i) in the topmost Fe layer, (ii) in the third Fe layer in the middle of the Fe film, (iii) in the interface Fe layer, (iv) in the interface Ir layer, and (v) in the bulk Ir. As it is apparent from Fig. 7(a), both spin-up and spin-down states of the interface Fe atoms are spread over a larger energy range, compared to the states of the Fe atoms sitting in the other Fe layers. In addition, a large

number of spin-up states exists near the Fermi level. Such states are absent in the DOS of the Fe atoms sitting in the topmost Fe layer and also in the DOS of the Fe atoms sitting in the middle of the Fe film [see Fig. 7(a)]. The orbital resolved DOS revealed that these states are mainly of d_{yz} and d_{xz} character. The two sharp peaks in the spin-up states of the surface Fe atoms at the energies of -1.9 and -2.7 eV are of d_{z^2} and d_{xz} (d_{yz}) character, respectively. These states are suppressed and slightly shifted in the DOS of interface Fe atoms. The spin-down density of states of the interface Fe atoms are also different from the ones of the Fe atoms sitting in the surface layer. The sharp surface state, located just slightly above the Fermi level, is not present in the spin-down DOS of the Fe atoms sitting in the interface Fe layer. Also the peak at about 0.7 eV, which is mainly of d_{z^2} character, is at much higher energies (1.3 eV) in the case of Fe atoms in the interface Fe layer. Comparing the density of states of the interface Ir atoms with the ones of the Ir atoms in the bulk Ir reveals that in the former case the spin-up states are at lower energies, whereas the spin-down states are at higher energies [see Fig. 7(b)]. All these facts are the indication of strong Fe $3d$ -Ir $5d$ electronic hybridizations at the Fe/Ir interface.

Second, we comment on the effect of the tetragonal distortion of the Fe film on the exchange interaction. At the Fe/Ir interface [see Fig. 6(b)], the interlayer exchange constants are slightly increased when a_{\perp} decreases from 3.20 Å (experimental value) to 2.86 Å (bulk value). In contrast, the intralayer exchange constants are slightly decreased. At the film surface, the interlayer exchange constants do not change too much considering the first two nearest neighbors [see Fig. 6(c)]. However, the intralayer exchange parameters are strongly suppressed with decreasing distance between Fe layers. This results in a softening of the magnons in such artificial structure [the blue (dashed) line in Fig. 5(b)]. This unusual relation has been discussed in the case of Fe(111)/Au/W(110) system and is attributed to the complexity of the electronic structure and the contribution of different orbitals to the exchange interaction [18].

It should be noted that the magnons are softer when the c/a ratio decreases from 1.16 to 1.04 . This is contradictory to the trend seen in the recent calculation for the FeCo bulk compounds with different tetragonal distortion [41], where a larger tetragonal distortion gives rise to a stronger magnon softening. However, in that work the volume of the unit cell is kept constant and the total spin magnetic moment of the unit cell is insensitive to the distortion. In our calculations, we decrease the interlayer distance but keep the in-plane lattice constant the same. The volume of the unit cell is then decreased and we found that the magnetic moments are also decreased by around 8% in average. Therefore, these two calculations are based on different assumptions and hence may not be directly compared.

B. 6–10 ML Fe

In Fig. 8, the magnon dispersion relation on the Fe films with thicknesses of 6–9 ML is shown. The symbols are the experimental data and the solid lines are the calculated results. The magnon dispersion relation does not change drastically when the thickness of the Fe film changes from 6 to 9 ML (the thickness range where the films are grown epitaxially and

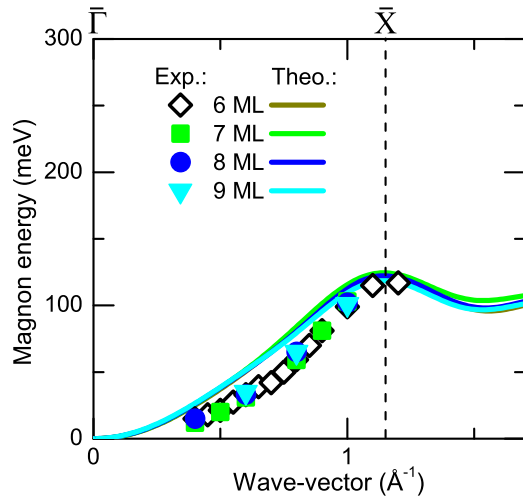


FIG. 8. (Color online) Magnon dispersion relation of 6 to 9 ML Fe grown on Ir(001) obtained at room temperature. The symbols represent the experimental data. The solid lines show the results of calculations.

are uniformly strained). The theoretical results also show the same trend.

In Fig. 9, the magnon energy and the corresponding asymmetry $[(I_{\downarrow} - I_{\uparrow})/(I_{\downarrow} + I_{\uparrow})]$ at that energy are plotted as a function of Fe thickness. The data are presented for $\Delta K_{\parallel} = 0.8 \text{ \AA}^{-1}$. The Kerr ellipticity at remanence divided by the thickness is also plotted as red open symbols in Fig. 9(b) for comparison. It is observed that once the film turns into the ferromagnetic state, the magnon energy stays nearly the same within the uniformly strained region. The value of the asymmetry may be regarded as the ferromagnetic signal of the sample. It shows the same behavior as the remanent magnetization measured by MOKE. The value of asymmetry increases from 5% for the 4.8 ML sample to 23% for the 6 ML sample and stays constant. This is the thickness where remanence and saturation become equal.

In the case of Fe films on W(110), a nonmonotonic thickness dependence of the magnon energies has been reported [19]. Combining the experimental and theoretical investigations, it is found that the chemical hybridizations with the substrate and the atomic relaxation in the film are both crucial for description of the experimental results. In that work, the atomically relaxed structure has been first considered, and then the case of atomically unrelaxed structure has been also calculated for comparison. It turned out that the relaxed one has a maximum of energy at 2 ML and gradually decreases, in line with the experimental observation. On the other hand, it is noticed that for the unrelaxed structure the magnon energy drastically increases from 1 to 2 ML but varies just slightly above 2 ML. The results of calculations for such cases are in agreement with the experiments on epitaxially grown Fe films on Ir(001).

As mentioned earlier in the case of 6 ML Fe/Ir(001) the main contribution to the low-energy magnon mode is coming from the Fe/Ir(001) interface [40]. Increasing the Fe thickness within the epitaxial growth region changes neither the interface layer nor the structure of the whole film. Therefore, the magnon dispersion relation within this thickness range does not change drastically.

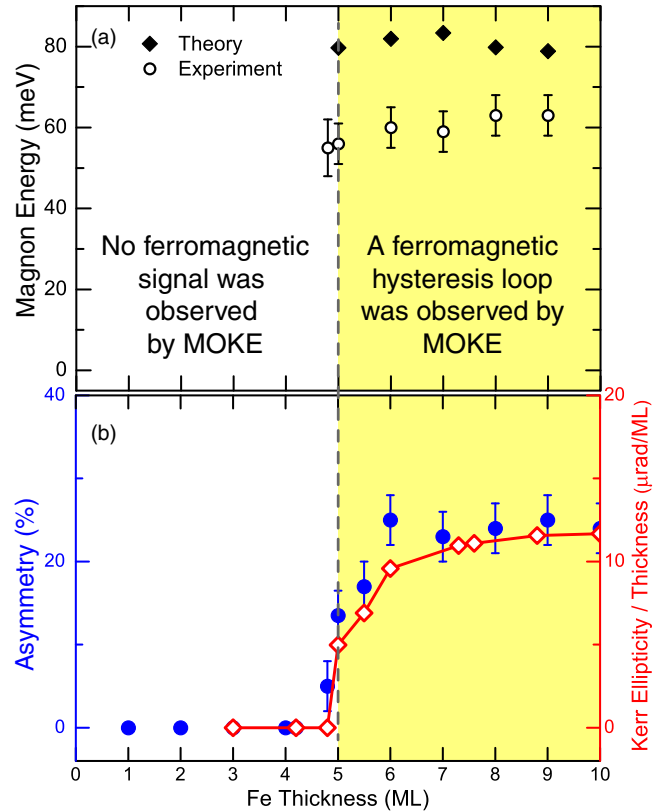


FIG. 9. (Color online) (a) Calculated (solid diamonds) and experimental (open circles) magnon energy at $\Delta K_{\parallel} = 0.8 \text{ \AA}^{-1}$ versus Fe thickness. (b) Blue solid circle: asymmetry $[(I_{\downarrow} - I_{\uparrow})/(I_{\downarrow} + I_{\uparrow})]$ at the magnon energy as a function of Fe thickness; red open symbols: Kerr ellipticity at remanence divided by the Fe thickness. The dashed line indicates the onset of the ferromagnetic order at room temperature, which is at 5 ML.

C. 10–27 ML Fe

According to the literature [25,26] and also our LEED experiments (Fig. 1), the Fe films start to relax when the thickness is above 10 ML. This effect has a direct consequence on the magnetic hysteresis loop [as seen in the MOKE measurements (Fig. 2)]. When the film starts to relax, the atomic structure may differ locally. This leads to the appearance of magnetic domains. Due to the random orientation of different magnetic domains, the remanent magnetization is small. This is supported by the results of the SPEELS measurements. It is observed that the difference intensity and the asymmetry measured on 13 and 17 ML Fe/Ir(001) are too small to be observed as a well-defined peak. This is due to the fact that the average magnetization direction is no longer perpendicular to the scattering plane (parallel or antiparallel to the polarization axis of the incoming electron beam). Starting from 19 ML, the difference intensity increases gradually, but it is still weak.

In Fig. 10, the magnon dispersion relation measured on thick Fe films (from 19 to 27 ML) is shown and compared to the one probed on a 6 ML sample. The surface Brillouin zone boundary of the relaxed films is at 1.10 \AA^{-1} if we take the lattice constant as the one of the bulk Fe ($a_0 = 2.866 \text{ \AA}$). Starting from 19 ML, the Fe film is totally relaxed to a bulklike

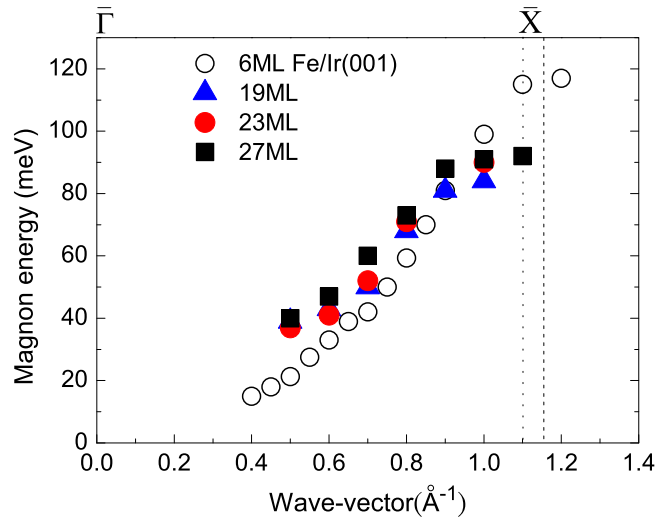


FIG. 10. (Color online) Magnon dispersion relation measured along the $\bar{\Gamma}$ - \bar{X} direction for thick Fe (> 10 ML) films grown on Ir(001) and compared to the one of 6 ML. The zone boundary of the relaxed film is at 1.10 \AA^{-1} shown as the dotted line, and the one of the 6 ML film is at 1.16 \AA^{-1} shown as the dashed line.

film. The magnon energies are similar to the results of our previous measurements performed on thick Fe films (24 ML) grown on W(110) up to $\Delta K_{\parallel} = 0.7 \text{ \AA}^{-1}$ [8]. The differences appear close to the zone boundary.

In Fig. 11, the magnon dispersion relation obtained on 27 ML Fe on Ir(001) and 24 ML Fe on W(110) [8] is shown as black squares and red circles, respectively. The magnon excitations in Fe films on Ir(001) are probed along the $\bar{\Gamma}$ - \bar{X} direction and the ones in the Fe films on W(110) are probed along the $\bar{\Gamma}$ - \bar{H} direction. The zone boundary is at 1.10 \AA^{-1} for

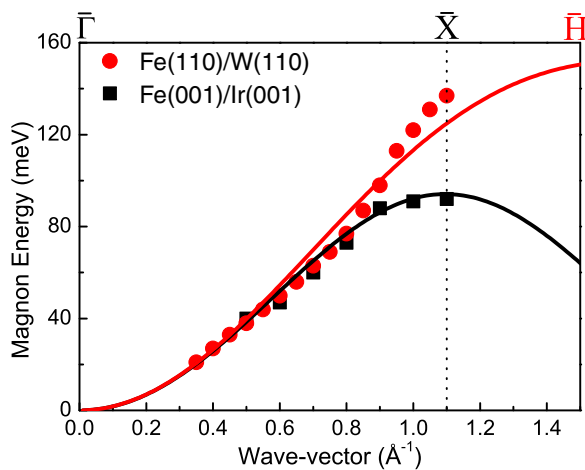


FIG. 11. (Color online) Magnon dispersion relation obtained on thick Fe films grown on different substrates with different surface orientations. The red circles are the experimental data measured on 24 ML Fe(110) grown on W(110) [8]. The black squares are the results of 27 ML Fe(001) on Ir(001). The error bars in energy are typically around 5 meV from 0.4 to 0.8 \AA^{-1} , and around 10 meV above 0.8 \AA^{-1} . The dispersion relation could be well described by the Heisenberg model using the same exchange parameters. The fit parameters are $J_{NS} = 6.8 \text{ meV}$ and $J_{NN} = 4.1 \text{ meV}$.

the $\bar{\Gamma}$ - \bar{X} direction and at 1.64 \AA^{-1} for the $\bar{\Gamma}$ - \bar{H} direction. The solid lines in Fig. 11 are the low-energy magnon mode in the Heisenberg model, where only the first and the second nearest neighbors are considered. Interestingly, the dispersion relation in both cases can be well fitted by using the same effective exchange parameters. The effective exchange constants for the first nearest neighbors and the second nearest neighbors are 6.8 meV and 4.1 meV, respectively. The energy difference between two dispersion relations is only due to different lengths of surface Brillouin zone boundaries. In both cases, the effective exchange parameters are smaller than the ones expected for bulk Fe according to the experimental data obtained from inelastic neutron scattering experiments [42]. This suggests that the effective exchange parameters at the surface of an Fe film are smaller than the ones in bulk Fe. It has been predicted by Turek *et al.*, based on the Heisenberg model, that the layer-resolved on-site exchange parameter of bcc Fe has a minimum at the top surface layer [43]. The reduction of the exchange parameters in the surface layer is due to the reduced coordination. However, it is in contrast to the results of *ab initio* electronic structure calculations, which predict that the interlayer exchange couplings derived from total-energy differences are enhanced at the surface for a semi-infinite slab [43].

It should be noted that in the case of epitaxial Fe films (< 10 ML) the main contribution to the lowest-lying mode is coming from the interface Fe layer. This is due to the relatively weak exchange interaction in the interface layer compared to the surface layer [40]. In the case of thick Fe films, which are relaxed to bulklike films, the main contribution to the observed magnon mode is coming from the surface layer [8].

The observation of the same effective exchange parameters on the thick Fe films grown on different substrates (W and Ir) is in agreement with the previous discussion. Since in both cases we mainly probe the surface magnons, the thickness of the Fe film is large enough to neglect the effects caused by the film/substrate interface. It should be noted that the surface orientations of the Fe film are different for these two cases. Turek *et al.* have also calculated the layer-resolved magnetic moments and the on-site exchange parameters on Fe(001) and Fe(110) surfaces [43]. It is found that the magnetic moment on the top surface layer of Fe(001) is larger than the one on the Fe(110) surface. However, the exchange parameter on the surface layer of Fe(001) is smaller than the one on Fe(110). Since we can only extract the quantity JS from our experimental results, a reduction of J may compensate the enhancement of S , and vice versa. Therefore, a similar JS would be expected on Fe(001) and Fe(110) surfaces.

In Ref. [22] the magnon dispersion relation of 3 and 4 ML Fe on Cu(001) is measured. After a comparison to the results of 24 ML Fe(110) on W(110), it has been concluded that the Fe films on Cu(001) grow in the so-called “nanomartensitic phase.” As one can see in Fig. 11, the magnon energies measured for different surface orientations of Fe films are almost identical at low and intermediate wave vectors. The differences appear only at high wave vectors close to the zone boundary. This means that only by comparing the magnon dispersion relation of two films, one cannot conclude that their atomic structure is the same, although the magnon energies might be identical.

The magnon dispersion relation of thick Fe films with different orientation shows similar energies at low wave-vector region, i.e., lower than 0.7 \AA^{-1} . The energies start to deviate at about 0.8 \AA^{-1} . This observation is in agreement with the Heisenberg model which predicts similar excitation energies for bcc Fe at low wave vectors. The differences appear close to the zone boundary due to the geometrical considerations, as for the (110) surface the length of the Brillouin zone is longer. For bulk Fe, this has been observed by Mook *et al.* by using inelastic neutron scattering [10]. In their measurements, the magnon dispersion relation is found to be similar for three main symmetry directions in bulk Fe up to 0.7 \AA^{-1} . At high wave vectors, the magnon intensity is too low to be measured. The low intensity is ascribed to the magnon damping into the Stoner continuum. In our experiments, the dispersion relation is measured up to 1.1 \AA^{-1} in both directions. Although the magnons at high wave vectors are strongly damped, the data quality is still very good and the energy difference between two directions for $\Delta K_{\parallel} > 0.9 \text{ \AA}^{-1}$ is clearly visible.

V. CONCLUSIONS

The experimentally measured magnon dispersion relation in Fe(001) films grown on Ir(001) is presented. The

experimental results are in good agreement with the *ab initio* calculations. Based on the comparison of experimental and theoretical results, we conclude that the strain induced distortion and the chemical hybridizations of the film and substrate are both crucial to understanding the magnetic excitations in this system. The magnon dispersion relation is measured for different thicknesses of Fe films where the film is uniformly strained (5–10 ML). It is found that the magnon dispersion relation does not change significantly when the film thickness is changed within the uniformly strained region. The magnon dispersion relation is also probed on relaxed Fe films. It is found that the magnon energies differ from the ones measured in thick Fe(110) films grown on W(110) only near the surface Brillouin zone boundary. However, the dispersion relation can be explained by taking the Heisenberg Hamiltonian and using the same values of exchange parameters.

ACKNOWLEDGMENTS

Funding from the Deutsche Forschungsgemeinschaft is acknowledged by A.E. (DFG priority program SPP 1538 “Spin Caloric Transport”). The calculations were performed at the Rechenzentrum Garching of the Max Planck Society (Germany).

-
- [1] C. Herring and C. Kittel, *Phys. Rev.* **81**, 869 (1951).
 - [2] M. Farle, *Rep. Prog. Phys.* **61**, 755 (1998).
 - [3] P. A. Grünberg, *Prog. Surf. Sci.* **18**, 1 (1985).
 - [4] B. Hillebrands, P. Baumgart, and G. Güntherodt, *Phys. Rev. B* **36**, 2450 (1987).
 - [5] M. Plihal, D. L. Mills, and J. Kirschner, *Phys. Rev. Lett.* **82**, 2579 (1999).
 - [6] Y. Zhang, T.-H. Chuang, K. Zakeri, and J. Kirschner, *Phys. Rev. Lett.* **109**, 087203 (2012).
 - [7] K. Zakeri, Y. Zhang, T.-H. Chuang, and J. Kirschner, *Phys. Rev. Lett.* **108**, 197205 (2012).
 - [8] K. Zakeri, Y. Zhang, and J. Kirschner, *J. Electron Spectrosc. Relat. Phenom.* **189**, 157 (2013).
 - [9] B. N. Brockhouse, *Phys. Rev.* **106**, 859 (1957).
 - [10] H. A. Mook and R. M. Nicklow, *Phys. Rev. B* **7**, 336 (1973).
 - [11] H. Ibach, D. Bruchmann, R. Vollmer, M. Etzkorn, P. S. A. Kumar, and J. Kirschner, *Rev. Sci. Instrum.* **74**, 4089 (2003).
 - [12] H. Ibach, J. Rajeswari, and C. M. Schneider, *Rev. Sci. Instrum.* **82**, 123904 (2011).
 - [13] H. Ibach and J. Rajeswari, *J. Electron Spectrosc. Relat. Phenom.* **185**, 61 (2012).
 - [14] R. Vollmer, M. Etzkorn, P. S. A. Kumar, H. Ibach, and J. Kirschner, *Phys. Rev. Lett.* **91**, 147201 (2003).
 - [15] W. X. Tang, Y. Zhang, I. Tudosa, J. Prokop, M. Etzkorn, and J. Kirschner, *Phys. Rev. Lett.* **99**, 087202 (2007).
 - [16] J. Prokop, W. X. Tang, Y. Zhang, I. Tudosa, T. R. F. Peixoto, K. Zakeri, and J. Kirschner, *Phys. Rev. Lett.* **102**, 177206 (2009).
 - [17] K. Zakeri, Y. Zhang, J. Prokop, T.-H. Chuang, N. Sakr, W. X. Tang, and J. Kirschner, *Phys. Rev. Lett.* **104**, 137203 (2010).
 - [18] T.-H. Chuang, K. Zakeri, A. Ernst, L. M. Sandratskii, P. Buczek, Y. Zhang, H. J. Qin, W. Adeagbo, W. Hergert, and J. Kirschner, *Phys. Rev. Lett.* **109**, 207201 (2012).
 - [19] Y. Zhang, P. Buczek, L. Sandratskii, W. X. Tang, J. Prokop, I. Tudosa, T. R. F. Peixoto, K. Zakeri, and J. Kirschner, *Phys. Rev. B* **81**, 094438 (2010).
 - [20] M. R. Verney and H. Hopster, *Phys. Rev. B* **68**, 132403 (2003).
 - [21] T. Komesu, G. D. Waddill, and J. G. Tobin, *J. Phys.: Condens. Matter* **18**, 8829 (2006).
 - [22] J. Rajeswari, H. Ibach, and C. M. Schneider, *Europhys. Lett.* **101**, 17003 (2013).
 - [23] J. Zarestky and C. Stassis, *Phys. Rev. B* **35**, 4500 (1987).
 - [24] M. Kottcke and K. Heinz, *Surf. Sci.* **376**, 352 (1997).
 - [25] V. Martin, W. Meyer, C. Giovanardi, L. Hammer, K. Heinz, Z. Tian, D. Sander, and J. Kirschner, *Phys. Rev. B* **76**, 205418 (2007).
 - [26] Z. Tian, D. Sander, and J. Kirschner, *Phys. Rev. B* **79**, 024432 (2009).
 - [27] J. Kudrnovský, F. Mácá, I. Turek, and J. Redinger, *Phys. Rev. B* **80**, 064405 (2009).
 - [28] A. Deák, L. Szunyogh, and B. Ujfalussy, *Phys. Rev. B* **84**, 224413 (2011).
 - [29] K. Zakeri, T. Peixoto, Y. Zhang, J. Prokop, and J. Kirschner, *Surf. Sci.* **604**, L1 (2010).
 - [30] K. Heinz, G. Schmidt, L. Hammer, and K. Müller, *Phys. Rev. B* **32**, 6214 (1985).
 - [31] L. Hammer, W. Meier, A. Klein, P. Landfried, A. Schmidt, and K. Heinz, *Phys. Rev. Lett.* **91**, 156101 (2003).
 - [32] K. Heinz and L. Hammer, *Prog. Surf. Sci.* **84**, 2 (2009).
 - [33] K. Zakeri and J. Kirschner, in *Topics in Applied Physics: Magnonics*, edited by S. O. Demokritov and A. N. Slavin (Springer-Verlag, Berlin, 2012), Chap. 7.
 - [34] J. Kessler, *Polarized Electrons* (Springer-Verlag, Berlin, 1985).
 - [35] J. Kirschner, *Phys. Rev. Lett.* **55**, 973 (1985).

- [36] L. Bergqvist, A. Taroni, A. Bergman, C. Etz, and O. Eriksson, *Phys. Rev. B* **87**, 144401 (2013).
- [37] J. P. Perdew, K. Burke, and M. Ernzerhof, *Phys. Rev. Lett.* **77**, 3865 (1996).
- [38] M. Lüders, A. Ernst, W. M. Temmerman, Z. Szotek, and P. J. Durham, *J. Phys.: Condens. Matter* **13**, 8587 (2001).
- [39] A. I. Liechtenstein, M. I. Katsnelson, V. P. Antropov, and V. A. Gubanov, *J. Magn. Magn. Mater.* **67**, 65 (1987).
- [40] K. Zakeri, T.-H. Chuang, A. Ernst, L. M. Sandratskii, P. Buczek, H. J. Qin, Y. Zhang, and J. Kirschner, *Nat. Nanotech.* **8**, 853 (2013).
- [41] E. Şaşıoğlu, C. Friedrich, and S. Blügel, *Phys. Rev. B* **87**, 020410(R) (2013).
- [42] J. W. Lynn, *Phys. Rev. B* **11**, 2624 (1975).
- [43] I. Turek, J. Kudrnovský, G. Bihlmayer, and P. Weinberger, *Czech. J. Phys.* **53**, 81 (2003).